Research Article | Vol. 29, No. 19 / 13 Sep 2021 / Optics Express 30809
Optics EXPRESS

Second-order statistical properties of conjugate mode "double-*H*" partially coherent beams in turbulence

RONG LIN,[1,2] JIDONG WU,[1] YIMING DONG,[3] GREG GBUR,[4,6] YANGJIAN CAI,[1,5,7] AND JIAYI YU[1,8]

[1]*Shandong Provincial Engineering and Technical Center of Light Manipulations & Shandong Provincial Key Laboratory of Optics and Photonic Device, School of Physics and Electronics, Shandong Normal University, Jinan 250014, China*
[2]*College of Physics and Electronics Engineering, Heze University, Heze 274015, China*
[3]*Department of Physics, Shaoxing University, Shaoxing 312000, China*
[4]*Department of Physics and Optical Science, University of North Carolina at Charlotte, Charlotte, North Carolina 28223, USA*
[5]*School of Physical Science and Technology, Soochow University, Suzhou 215006, China*
[6]*gjgbur@uncc.edu*
[7]*yangjiancai@suda.edu.cn*
[8]*jiayiyu0528@sdnu.edu.cn*

Abstract: We present an analysis of the propagation properties of a recently introduced class of conjugate mode partially coherent beams (called "double-*H*" beams) in a turbulent atmosphere using the extended Huygens-Fresnel integral. We investigate how the phase constant φ_0 between the modes plays a role in controlling the evolution of the intensity distribution and resisting the degradation effects of the atmosphere. Our results indicate that this new class of structured beams provides a new degree of freedom for controlling the shape of the beams and improves turbulence resistance, with potential application in free-space optical communications.

1. Introduction

Spatial coherence is one of the fundamental properties of a light field and it affects numerous propagation characteristics of such fields, including their directionality [1], spectrum [2], and degree of polarization [3,4]. Optical coherence theory has been well developed over the past few decades [5] and laser beams with decreased spatial coherence, labeled partially coherent beams (PCBs), have found advantages in many applications [6,7]. Free-space optical communications is one of the leading applications, and it is now recognized that using PCBs as a carrier in optical communications is an effective means to suppress turbulence-induced negative effects, and that PCBs can perform better than their fully coherent counterparts [8,9].

Studies of PCBs in atmospheric turbulence date back to the invention of the laser, but it is only in recent decades that they have become an intense focus of research. In 2002, G. Gbur and E. Wolf theoretically studied the mean squared width of PCBs in a random medium and their results suggested that there are circumstances where PCBs perform better than comparable coherent beams [8]. Subsequent experiments by A. Dogariu and S. Amarande confirmed this conclusion [10]. These reports, among others, greatly promoted research into the propagation characteristics of PCBs in turbulence. The resistance of PCBs to turbulence can be explained physically by use of the coherent mode representation, which indicates that light is sent simultaneously through distinct non-interfering channels, increasing the average light at the detector and reducing interference-based fluctuations [8,11].

Since the turn of the century, numerous reports have been published on how various classes of PCBs propagate, both in free space and in turbulence. Such beams are usually categorized

#434242 https://doi.org/10.1364/OE.434242
Journal © 2021 Received 16 Jun 2021; revised 18 Aug 2021; accepted 31 Aug 2021; published 9 Sep 2021

Optics EXPRESS

as conventional or non-conventional; for a conventional beam, the degree of coherence (DOC) has a homogeneous Gaussian distribution [12]. The propagation characteristics of beams of the conventional class in turbulence are similar, although the short range propagation of the beam can depend strongly on the initial beam profile, phases and state of polarization. However, when the beam propagates over a long range in free-space or turbulence, the intensity distribution gradually degenerates into a Gaussian distribution, independent of the initial intensity distribution.

Because of the restrictive behavior of conventional PCBs, lots of recent effort has focused on investigating the propagation characteristics of non-conventional PCBs. In 2007, Gori *et al.* proposed a new method for designing a wide variety of PCBs with novel and non-conventional correlation structures [13]. These beams can display a number of unusual characteristics at short propagation distances, such as self-focusing and transverse acceleration. Over long propagation distances in turbulence, the intensity profile of a non-conventional PCB still gradually degenerates into a Gaussian distribution; nevertheless, it can exhibit stronger turbulence resistance than a conventional PCB or coherent beam [12].

Though many new classes of beams have been developed using the formalism of Gori *et al.*, investigations have still not exhausted all the possibilities that the formalism has made available. To understand this, we note that the cross-spectral density (CSD) of a non-conventional PCB may be written in the source plane, according to Ref. [13], as

$$W(\mathbf{r}_1, \mathbf{r}_2) = \int p(\nu) H^*(\mathbf{r}_1, \nu) H(\mathbf{r}_2, \nu) d\nu, \tag{1}$$

where $p(\nu)$ is a non-negative probability density and $H(\mathbf{r}, \nu)$ represents a kernel of the integral. Equation (1) may be interpreted as an average over an ensemble of coherent fields $H(\mathbf{r}, \nu)$, where ν is a random variable (or set of random variables) and $p(\nu)$ is the probability density of the ensemble. Different combinations of $p(\nu)$ and $H(\mathbf{r}, \nu)$ can be used to generate various PCBs with different correlation structures [13–15]. However, in all of these examples, the choice of $H(\mathbf{r}, \nu)$ was limited to the simple form,

$$H(\mathbf{r}, \nu) = \tau(\mathbf{r}) \exp[ig(\boldsymbol{r})\nu], \tag{2}$$

with $g(\boldsymbol{r})$ being a real function and $\tau(\mathbf{r})$ an amplitude envelope; this form is commonly used because it is straightforward to generate experimentally [16–19]. For this class of PCBs, the kernel consists of a single term, and we refer to this as the class of "single-H PCBs."

It is clear that there are many other possibilities for kernels, including sums of distinct kernels that represent different coherent field modes. We refer to the class of PCBs using a sum of two kernels as "double-H PCBs," and focus in particular on a sum of two modes that are complex conjugates of each other,

$$H(\mathbf{r}, \nu) = \tau(\mathbf{r}) \left\{ \exp[ig(\boldsymbol{r})\nu + i\varphi_0] + \exp[-ig(\boldsymbol{r})\nu - i\varphi_0] \right\}, \tag{3}$$

where φ_0 is a constant phase parameter. This class was recently introduced in Ref. [20], which focused on the theoretical and experimental generation of such beams but did not discuss their propagation characteristics. The use of conjugate mode pairs in a kernel may be thought of as a rough analogy to the use of cylindrical vector beams in atmospheric propagation [21], where coherent combinations of beams with opposite orbital and spin angular momentum showed improved turbulence resistance.

In this paper, we report what is to our knowledge the first research discussing the propagation properties of the new beams, with emphasis on the effect of the new initial beam parameter, the phase constant φ_0, on the beam evolution and its resistance to turbulence.

Optics EXPRESS

2. Cross-spectral density of double-*H* PCBs propagating in turbulence

We now restrict ourselves to the case $g(\mathbf{r}) = r^2$ and $p(\nu)$ is a Gaussian distribution. As shown in Ref. [20], the CSD of double-H PCBs in the source plane can be evaluated to the form,

$$W(\boldsymbol{r}_1, \boldsymbol{r}_2) = \tau^*(\boldsymbol{r}_1)\tau(\boldsymbol{r}_2) \exp\left[-\frac{\left(\boldsymbol{r}_1^2 - \boldsymbol{r}_2^2\right)^2}{4\delta_g^4}\right]\left[1 + \exp\left(-\frac{\boldsymbol{r}_1^2\boldsymbol{r}_2^2}{\delta_g^4}\right)\cos\left(2\varphi_0\right)\right], \tag{4}$$

where $\boldsymbol{r}_1$ and $\boldsymbol{r}_2$ are two transverse position vectors in the source plane. The amplitude function $\tau(\boldsymbol{r})$ is taken to be a Gaussian, $\tau(\boldsymbol{r}) = \exp(-\boldsymbol{r}^2/w^2)$, where w is the beam width. The quantity δ_g represents the correlation length of the field and φ_0 is a phase constant.

As seen in Ref. [20] or Eq. (4), different choices of the phase constant φ_0 (limited $0 \le \varphi_0 \le \pi/2$, due to the periodicity of the cosine function) result in different classes of sources. When $\varphi_0 = \pi/4$, the sources reduce to a well know single-H source, the non-uniformly correlated (NUC) class, introduced by Lajunen *et al.* in 2011 [22], and reduce to the cosh- and sinh-type NUC sources of Ref. [20] when $\varphi_0 = 0$ and $\varphi_0 = \pi/2$, respectively. Hereafter, we will focus on discussing the second-order propagation characteristics of such sources on propagation and how they depend on the phase constant φ_0. Of course, this discussion is not limited to the comparison of NUC sources, cosh-type NUC sources and sinh-type NUC sources, but all cases of double-H sources.

To study the propagation characteristics of the field in turbulence, we assume paraxial propagation along the z-axis. Then, the CSD of a PCB traveling through a turbulent medium can be described by the extended Huygens-Fresnel integral [23],

$$\begin{aligned} W\left(\boldsymbol{\rho}_1, \boldsymbol{\rho}_2, z\right) = \frac{1}{\lambda^2 z^2}\iint_{-\infty}^{\infty} W_0\left(\boldsymbol{r}_1, \boldsymbol{r}_2\right) \exp\left[-\frac{ik}{2z}\left(\boldsymbol{r}_1 - \boldsymbol{\rho}_1\right)^2 + \frac{ik}{2z}\left(\boldsymbol{r}_2 - \boldsymbol{\rho}_2\right)^2\right] \\ \times \left\langle \exp\left[\Psi\left(\boldsymbol{r}_1, \boldsymbol{\rho}_1\right) + \Psi^*\left(\boldsymbol{r}_2, \boldsymbol{\rho}_2\right)\right]\right\rangle d^2\boldsymbol{r}_1 d^2\boldsymbol{r}_2, \end{aligned} \tag{5}$$

where $k = 2\pi/\lambda$ is the wavenumber and λ the wavelength. The vectors $\boldsymbol{\rho}_1$ and $\boldsymbol{\rho}_2$ are two arbitrary transverse position vectors in the target plane, $W_0(\boldsymbol{r}_1, \boldsymbol{r}_2)$ denotes the CSD of the beam in the source plane, and $\Psi(\boldsymbol{r}, \boldsymbol{\rho})$ is the complex phase perturbation induced by the refractive-index fluctuations of the turbulent medium between $\boldsymbol{r}$ and $\boldsymbol{\rho}$. The brackets $< \cdots >$ denote an ensemble average over the turbulence, and the average can be expressed as [23]

$$\begin{aligned} &\left\langle \exp\left[\Psi\left(\boldsymbol{r}_1, \boldsymbol{\rho}_1\right) + \Psi^*\left(\boldsymbol{r}_2, \boldsymbol{\rho}_2\right)\right]\right\rangle = \\ &\exp\left\{-\left(\frac{\pi^2 k^2 z}{3}\right)\left[\left(\boldsymbol{\rho}_1 - \boldsymbol{\rho}_2\right)^2 + \left(\boldsymbol{\rho}_1 - \boldsymbol{\rho}_2\right)\cdot\left(\boldsymbol{r}_1 - \boldsymbol{r}_2\right) + \left(\boldsymbol{r}_1 - \boldsymbol{r}_2\right)^2\right]\int_0^{\infty} \boldsymbol{\kappa}^3 \Phi_n\left(\boldsymbol{\kappa}\right) d^2\boldsymbol{\kappa}\right\}, \end{aligned} \tag{6}$$

where $\Phi_n(\boldsymbol{\kappa})$ is the spatial power spectrum of the refractive-index fluctuations of the turbulent medium. For brevity, we set

$$T = \int_0^{\infty} \boldsymbol{\kappa}^3 \Phi_n\left(\boldsymbol{\kappa}\right) d^2\boldsymbol{\kappa}. \tag{7}$$

We choose the von Karman power spectrum as the turbulence model, which can describe both Komogorov ($\alpha = 11/3$) and non-Kolmogorov ($\alpha \neq 11/3$) turbulence with inner and outer scales [24],

$$\Phi_n\left(\boldsymbol{\kappa}\right) = A\left(\alpha\right) C_n^2 \left(\kappa^2 + \kappa_0^2\right)^{-\alpha/2} \exp\left(-\kappa^2/\kappa_m^2\right). \tag{8}$$

With this turbulence spectrum, T can be expressed in the following form [24],

$$T = \frac{A(\alpha)}{2(\alpha - 2)} C_n^2 \left[\beta\kappa_m^{2-\alpha} \exp\left(\kappa_0^2/\kappa_m^2\right)\Gamma_1\left(2 - \alpha/2, \kappa_0^2/\kappa_m^2\right) - 2\kappa_0^{4-\alpha}\right], 3<\alpha<4, \tag{9}$$

where C_n^2 is a generalized refractive-index structure parameter, $\beta = 2\kappa_0^2 - 2\kappa_m^2 + \alpha\kappa_m^2$, $\kappa_0 = 2\pi/L_0$ with L_0 being the outer scale of turbulence, $\kappa_m = c(\alpha)/l_0$ with l_0 being the inner scale of

Optics EXPRESS

turbulence, $\Gamma_1(\cdot)$ is the incomplete Gamma function, and

$$A(\alpha) = \frac{1}{4\pi^2}\Gamma(\alpha-1)\cos(\alpha\pi/2), \quad c(\alpha) = \left[\frac{2\pi A(\alpha)}{3}\Gamma\left(\frac{5-\alpha}{2}\right)\right]^{1/(\alpha-5)}, \tag{10}$$

with $\Gamma(\cdot)$ denoting the Gamma function.

We may derive the CSD of double-H PCBs in the receiver plane using the above equations. However, it is too difficult to integrate directly by inserting Eq. (4) into Eq. (5). Expressing the beam model in the form of Eq. (1) and then interchanging the orders of the integrals, we obtain the formula

$$W(\boldsymbol{\rho}_1, \boldsymbol{\rho}_2, z) = \int p(v) P(\boldsymbol{\rho}_1, \boldsymbol{\rho}_2, v, z)\, dv, \tag{11}$$

where $P(\boldsymbol{\rho}_1, \boldsymbol{\rho}_2, v, z)$ is defined as

$$\begin{aligned} P(\boldsymbol{\rho}_1, \boldsymbol{\rho}_2 v, z) = \left(\frac{k}{2\pi z}\right)^2 \iint_{-\infty}^{\infty} H^*(\boldsymbol{r}_1, v) H(\boldsymbol{r}_2, v) \exp\left[-\frac{ik}{2z}(\boldsymbol{r}_1 - \boldsymbol{\rho}_1)^2 + \frac{ik}{2z}(\boldsymbol{r}_2 - \boldsymbol{\rho}_2)^2\right] \\ \times \langle \exp[\Psi^*(\boldsymbol{r}_1, \boldsymbol{\rho}_1) + \Psi(\boldsymbol{r}_2, \boldsymbol{\rho}_2)]\rangle\, d^2\boldsymbol{r}_1 d^2\boldsymbol{r}_2, \end{aligned} \tag{12}$$

and $H(\boldsymbol{r}, v)$ is the arbitrary kernel and $p(v)$ is the weighting function as shown in Eq. (3) above and Eq. (5) in Ref. [20].

After a lengthy integration, one obtains

$$P(\boldsymbol{\rho}_1, \boldsymbol{\rho}_2, v, z) = \left(\frac{k}{2\pi z}\right)^2 \exp\left[-\frac{ik}{2z}\left(\boldsymbol{\rho}_1^2 - \boldsymbol{\rho}_2^2\right)\right] \exp\left[-T'(\boldsymbol{\rho}_1 - \boldsymbol{\rho}_2)^2\right] \Theta, \tag{13}$$

where

$$\begin{aligned} \Theta = \pi^2 \exp\left(\frac{\mathfrak{R}_1^2}{4\Omega_1}\right)\left\{\frac{1}{\xi_1}\exp\left[\frac{\left(\mathfrak{R}_2 + \prod \Omega_1^{-1}/4\right)^2}{4\left(\Omega_1^* - T'^2\Omega_1^{-1}\right)}\right] + \frac{1}{\xi_3}\exp\left[\frac{\left(\mathfrak{R}_2 + \prod \Omega_1^{-1}/4\right)^2}{4\left(\Omega_2^* - T'^2\Omega_1^{-1}\right)}\right]\right\}\exp(-2i\varphi_0) \\ + \pi^2 \exp\left(\frac{\mathfrak{R}_1^2}{4\Omega_2}\right)\left\{\frac{1}{\xi_2}\exp\left[\frac{\left(\mathfrak{R}_2 + \prod \Omega_2^{-1}/4\right)^2}{4\left(\Omega_2^* - T'^2\Omega_2^{-1}\right)}\right] + \frac{1}{\xi_3^*}\exp\left[\frac{\left(\mathfrak{R}_2 + \prod \Omega_2^{-1}/4\right)^2}{4\left(\Omega_1^* - T'^2\Omega_2^{-1}\right)}\right]\right\}\exp(2i\varphi_0), \end{aligned} \tag{14}$$

with

$$T' = \frac{1}{3}\pi^2 k^2 z T; \quad \prod = \frac{4ikT'\rho_1}{z} - 4T'^2(\rho_1 - \rho_2); \tag{15}$$

$$\Omega_1 = \frac{1}{w^2} + \frac{ik}{2z} + iv + T'; \quad \Omega_2 = \frac{1}{w^2} + \frac{ik}{2z} - iv + T'; \tag{16}$$

$$\mathfrak{R}_1 = \frac{ik}{z}\rho_1 - T'(\rho_1 - \rho_2); \quad \mathfrak{R}_2 = -\frac{ik}{z}\rho_2 + T'(\rho_1 - \rho_2); \tag{17}$$

$$\xi_1 = \left(\frac{1}{w^2} + T'\right)^2 - \left(\frac{ik}{2z} + iv\right)^2 - T'^2; \tag{18}$$

$$\xi_2 = \left(\frac{1}{w^2} + T'\right)^2 - \left(\frac{ik}{2z} - iv\right)^2 - T'^2; \tag{19}$$

$$\xi_3 = \left(\frac{1}{w^2} + T' + iv\right)^2 - \left(\frac{ik}{2z}\right)^2 - T'^2. \tag{20}$$

Thus, we obtain the CSD of double-H PCBs after propagation in turbulence by evaluating the integral in Eq. (11). We then obtain the spectral intensity of such beams in the target plane from

Optics EXPRESS

the definition,

$$S(\boldsymbol{\rho}, z) = W(\boldsymbol{\rho}, \boldsymbol{\rho}, z). \tag{21}$$

The spectral DOC in the target plane is obtained from

$$\mu(\boldsymbol{\rho}_1, \boldsymbol{\rho}_2, z) = \frac{W(\boldsymbol{\rho}_1, \boldsymbol{\rho}_2, z)}{\sqrt{W(\boldsymbol{\rho}_1, \boldsymbol{\rho}_1, z) W(\boldsymbol{\rho}_2, \boldsymbol{\rho}_2, z)}}. \tag{22}$$

We may now explore the propagation properties of double-H PCBs in turbulent atmosphere by using the above formulas. In the limiting case $T = 0$, our formulas reduce to the case of beam propagation in free space.

3. Propagation factor and beam wander of double-*H* PCBs

The physics of PCB propagation in turbulence is complicated, and there are a wide variety of properties that one can analyze to assess the effect of the turbulence on PCBs. The most straightforward approach is to study global parameters of the beam, such as the propagation factor M^2 and the beam wander $\langle r_c^2 \rangle$; these can be calculated from the CSD of the source and can be expressed in terms of the second-order moments of the beams. In this section, we first derive the analytical expressions for the second-order moments of double-H PCBs in turbulence, and then derive the expressions for the propagation factor and beam wander of such beams in turbulence. These global parameters give an overall picture of the effect of turbulence on the beam propagation, which we then study in more detail in the following sections.

The second-order moments of the beams in turbulence in the target plane are obtained from the expressions [25],

$$\langle r^2 \rangle = \langle r^2 \rangle_0 + 2 \langle \boldsymbol{r} \cdot \boldsymbol{\theta} \rangle_0 z + \langle \theta^2 \rangle_0 z^2 + \frac{4}{3} \pi^2 T z^3, \tag{23}$$

$$\langle \theta^2 \rangle = \langle \theta^2 \rangle_0 + 4\pi^2 T z, \tag{24}$$

$$\langle \boldsymbol{r} \cdot \boldsymbol{\theta} \rangle = \langle \boldsymbol{r} \cdot \boldsymbol{\theta} \rangle_0 + \langle \theta^2 \rangle_0 z + 2\pi^2 T z^2, \tag{25}$$

where $\boldsymbol{r} = (x, y)$ and $\boldsymbol{\theta} = (\theta_x, \theta_y)$, $r = |\boldsymbol{r}|$ and $\theta = |\boldsymbol{\theta}|$. The quantities $\langle r^2 \rangle_0$, $\langle \boldsymbol{r} \cdot \boldsymbol{\theta} \rangle_0$ and $\langle \theta^2 \rangle_0$ denote the second-order moments of a PCB in source plane and they can be obtained by the integrals [26],

$$\langle r^2 \rangle_0 = \frac{1}{I} \int_0^{2\pi} \int_0^{\infty} r^3 W(r, \theta, r, \theta) dr d\theta, \tag{26}$$

$$\langle \theta^2 \rangle_0 = \frac{1}{k^2 I} \int_0^{2\pi} \int_0^{\infty} \left\{ \frac{\partial^2 W(r_1, \theta_1, r_2, \theta_2)}{\partial r_1 \partial r_2} \bigg|_{\theta_1 = \theta_2 = \theta}^{r_1 = r_2 = r} + \frac{1}{r^2} \frac{\partial W(r_1, \theta_1, r_2, \theta_2)}{\partial \theta_1 \partial \theta_2} \bigg|_{\theta_1 = \theta_2 = \theta}^{r_1 = r_2 = r} \right\} r dr d\theta, \tag{27}$$

$$\langle \boldsymbol{r} \cdot \boldsymbol{\theta} \rangle_0 = \frac{1}{ikI} \int_0^{2\pi} \int_0^{\infty} \left\{ r_1 \frac{\partial W(r_1, \theta_1, r_2, \theta_2)}{\partial r_1} - r_2 \frac{\partial W(r_1, \theta_1, r_2, \theta_2)}{\partial r_2} \right\} \bigg|_{\theta_1 = \theta_2 = \theta}^{r_1 = r_2 = r} r dr d\theta. \tag{28}$$

In these expressions, I represents the integrated intensity of the beams, i.e.,

$$I = \int_0^{2\pi} \int_0^{\infty} W(r, \theta, r, \theta; 0) r dr d\theta. \tag{29}$$

The second-order moments mentioned above allow us to evaluate the beam quality parameter, defined as [27]

$$Q = \langle \rho^2 \rangle \langle \theta^2 \rangle - \langle \boldsymbol{\rho} \cdot \boldsymbol{\theta} \rangle^2 \tag{30}$$

This parameter is related to the beam propagation factor M^2 through the expression $M^2 = \sqrt{Q}$. A better beam quality is associated with a smaller beam divergence and a consequently smaller M^2, for a fixed beam width at the source plane.

Optics EXPRESS

The beam wander may also be used to characterize the effects of turbulence on PCB propagation. It can described statistically as the variance of the displacement of the instantaneous center of the beam as it propagates through turbulence. A model of beam wander valid under all turbulence conditions is given by Andrews and Phillips as [28]

$$\left\langle r_c^2 \right\rangle = 4\pi^2 k^2 W_{FS}^2 \int_0^L \int_0^\infty \kappa \Phi_n(\kappa) H_{LS}(\kappa, z) \left\{ 1 - \exp\left[-\frac{\Lambda L \kappa^2 (1 - z/L)^2}{k} \right] \right\} d\kappa dz, \tag{31}$$

where L is the total propagation path length, and z is the distance of an intercept point from the input plane. $\Lambda = 2L/kW_{FS}^2$ with W_{FS} is the beam width at the receiver plane in the absence of turbulence. The quantity $H_{LS}(\kappa, z) = \exp(-\kappa^2 W_{LT}^2)$ is a large-scale filter function and W_{LT} is the long-term beam width in the presence of turbulence.

Using a geometrical optics approximation in which diffraction effects are neglected, and the model of turbulence chosen in Eq. (8), we can integrate Eq. (31) and obtain a formula for the beam wander in turbulence,

$$\begin{aligned} \left\langle r_c^2 \right\rangle = {} & \frac{4\pi^2 C_n^2 A(\alpha) L^2}{(\alpha - 2)} \kappa_0^{-\alpha} \int_0^L \left(1 - \frac{z}{L}\right)^2 \left\{ -2\kappa_0^4 + \kappa_0^\alpha \kappa_m^2 \left(W_{LT}^2 + \kappa_m^{-2} \right)^{\alpha/2} \right. \\ & \times \left(1 + \kappa_m^2 W_{LT}^2\right)^{-2} \left[2\kappa_0^2 \left(1 + \kappa_m^2 W_{LT}^2\right) + (\alpha - 2)\kappa_m^2 \right] \exp\left[\left(\frac{\kappa_0}{\kappa_m} \right)^2 + \kappa_0^2 W_{LT}^2 \right] \\ & \left. \times \Gamma\left[2 - \frac{\alpha}{2}, \left(\frac{\kappa_0}{\kappa_m} \right)^2 + \kappa_0^2 W_{LT}^2 \right] \right\} dz. \end{aligned} \tag{32}$$

It is worth noting that the beam wander depends on the source parameters – the only parameters we can control – only through the long-term beam width W_{LT}. Any change to the source parameters that affects W_{LT} will consequently affect beam wander, and W_{LT} can depend on these parameters in a non-trivial way. The quantity W_{LT} can be described as the mean-squared beam width $\left\langle r^2 \right\rangle$ of a laser beam propagating in turbulence [26], which can be obtained from Eq. (23) above.

Therefore, in general, we can study the properties of propagation factor and beam wander by using Eqs. (23–25) and Eq. (30) and Eq. (32).

4. Statistical properties of double-*H* PCBs

Using the formulas we derived in above section, we next study the statistical properties of double-*H* PCBs in source plane and after propagation in free space and in turbulence. In the following calculations, we use the following beam and turbulence parameters: $\lambda = 632.8$nm, $w = 3$cm, $L_0 = 1$m, $l_0 = 1$mm, $\alpha = 11/3$ and $C_n^2 = 10^{-15}\mathrm{m}^{-2/3}$.

4.1. In the source plane

The spectral intensity distributions for different choices of the phase constant φ_0 and correlation length δ_g of the proposed double-*H* sources are shown in Fig. 1 . One can see that the beam profile varies significantly with changes to the two initial beam parameters, the phase constant φ_0 and the coherence length δ_g. Figures 1(a1-5) show that when $\varphi_0 < \pi/4$, the spectral density displays a bright, axially symmetric core, and the size of the bright core decreases with increasing phase constant. Figures 1(b1-5) illustrate how the correlation length affects the core behavior. While the spectral density exhibits the the dark core when $\varphi_0 > \pi/4$, it becomes deeper and narrower with increasing phase constant and/or decreasing coherence. The beam profile remains Gaussian distribution and is independent of the value of coherence parameter δ_g when phase constant $\varphi_0 = \pi/4$; in this case, the double-*H* source is reduced to a conventional NUC source, which was discussed in detail in Ref. [22,29].

Optics EXPRESS

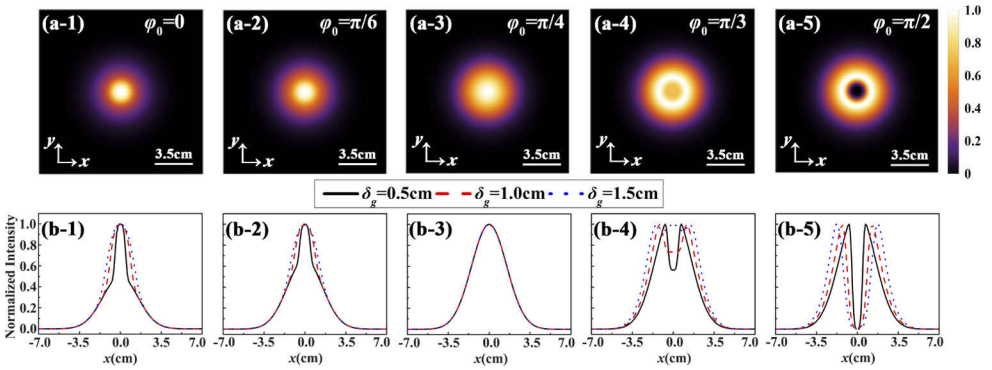

Fig. 1. Density plot of the normalized intensity and the corresponding cross-line of double-H source for different phase constants φ_0 and coherence lengths δ_g. In Figures (a1-5), δ_g = 1.0cm.

Figure 2 shows the density plot of the modulus of the DOC and corresponding cross-lines of double-H sources for different values of the phase constant φ_0. We find that the coherence of double-H sources also exhibits striking effects. Figure 2(a) shows the high-coherence area of such sources is confined to the center and on two diagonal lines in the source plane. When the value of phase constant increases to $\pi/4$, the coverage of the high-coherence area in center reduces and evolves into an "X" distribution, after which the high-coherence area in center increases gradually to a rectangular like distribution. It is worth mentioning that the value of the DOC on both lines ($r_1 = 0$ and $r_2 = 0$) is 0 (except the point DOC($r_1 = r_2 = 0$) = 1) when $\varphi_0 = \pi/2$. This feature is difficult to see in the cross-sectional plots, so Figs. 2(b) and 2(c) show the cross-lines $|\boldsymbol{\mu}|\,(r_2 = 0)$ and $|\boldsymbol{\mu}|\,(r_2 = \delta_g)$. We confirm that the high-coherence area decreases first and then increases versus the increasing phase constant. We therefore have a class of double-H sources with distinct correlation functions and the spatial coherence develops extreme changes as $\varphi_0 \to \pi/2$.

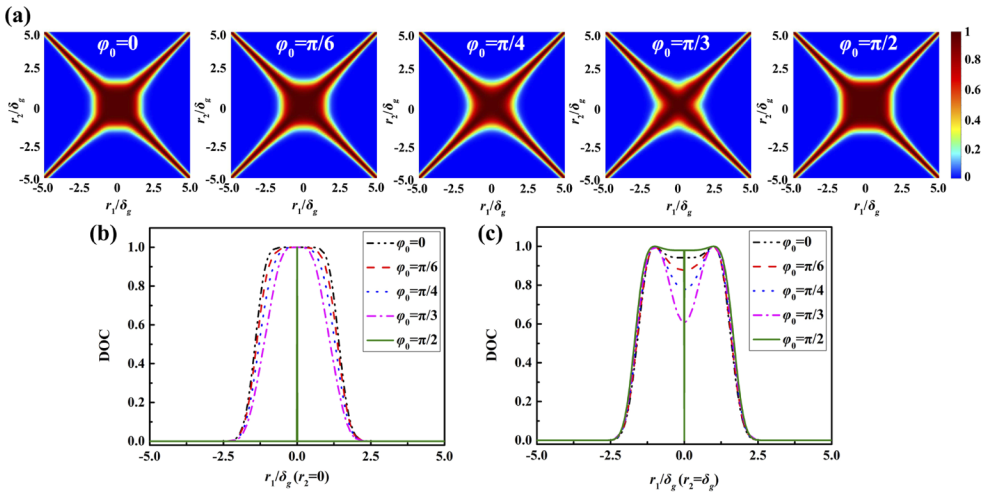

Fig. 2. (a) Density plot of the modulus of the DOC and corresponding cross-line (b) $|\boldsymbol{\mu}|\,(r_2 = 0)$, (c) $|\boldsymbol{\mu}|\,(r_2 = \delta_g)$ of double-H sources for different phase constant φ_0.

Optics EXPRESS

4.2. Propagation in free space

Figure 3 shows the normalized intensity and corresponding cross-line of double-H PCBs at different distances in free space with different phase constants φ_0. The evolution of spectral density shows that such beams all display self-focusing properties, just as the conventional NUC beams ($\varphi_0 = \pi/4$) do. When the phase constant $\varphi_0 < \pi/4$, the size of the bright core decreases at short propagation distances, and increases at long propagation distances. In the case of $\varphi_0 > \pi/4$, double-H PCBs evolve in a non-trivial way. A new extremely small bright core appears in the center of the beams and the small bright core grows in size and intensity during propagation, gradually evolving to a Gaussian beam profile, while the outside ring diminishes and disappears.

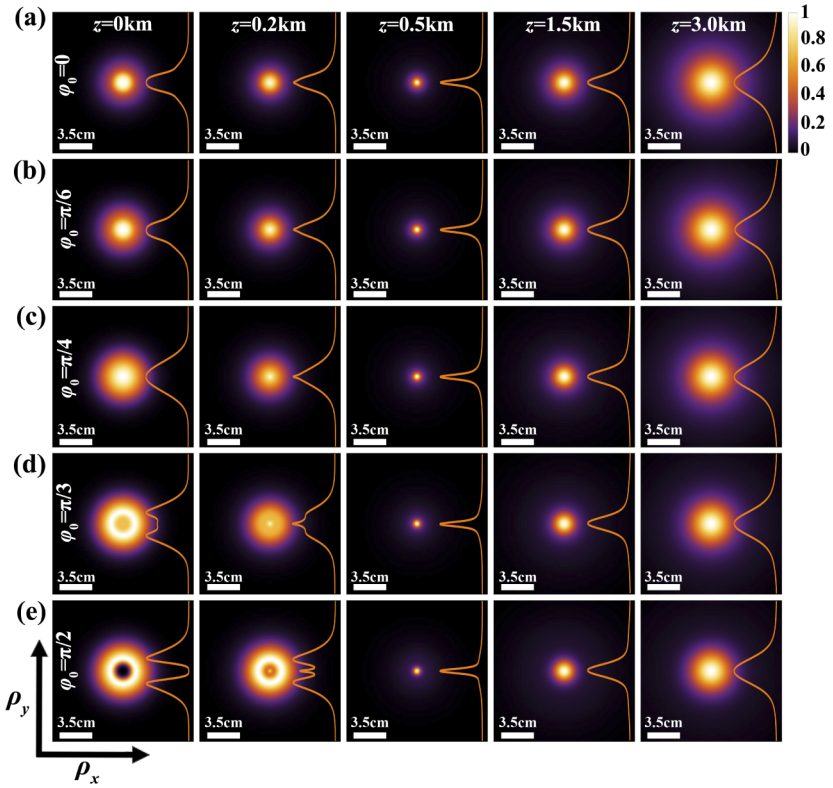

Fig. 3. The normalized intensity of double-H PCBs upon propagation in free space for different phase constant with coherence length δ_g=1cm.

We may interpret this result by looking again at the definition of the double-H kernel, Eq. (3). When $g(\mathbf{r}) = r^2$, our kernel consists of a coherent superposition of terms with positive and negative wavefront curvatures, which causes them to converge at different focal distances given by the expression $z = 1/2v$. On propagation, the positive curvature contribution will tend to diverge, while the negative curvature contribution will focus. With $\varphi_0 > \pi/4$, these two fields are out of phase, resulting in the beam's dark core. In essence, our double-H beams represent a new form of dark hollow beam [30] which is partially coherent, and whose propagation characteristics depend on the statistical properties of the beam.

In order to show more clearly the effects of the phase constant φ_0 and coherence length δ_g on the self-focusing properties of such beams, we characterize the ratio of the maximum intensity of double-H PCBs on the axis on propagation to the intensity on the axis at the source plane, i.e. $S_{\max}(0, z)/S(0, 0)$. We determine from Fig. 4 that the ratio increases slowly over small phase

Optics EXPRESS

constant ranges, but when the value of phase constant φ_0 is larger than about $\pi/3$, the ratio increases sharply, and it approaches infinity as the phase constant φ_0 is $\pi/2$, which is because such beams with $\varphi_0 = \pi/2$ at source plane have a perfect dark hollow core, making $S(0, 0) = 0$. One confirms that the self-focusing property (ratio value) of double-H PCBs with larger phase constant φ_0 and lower coherence is stronger.

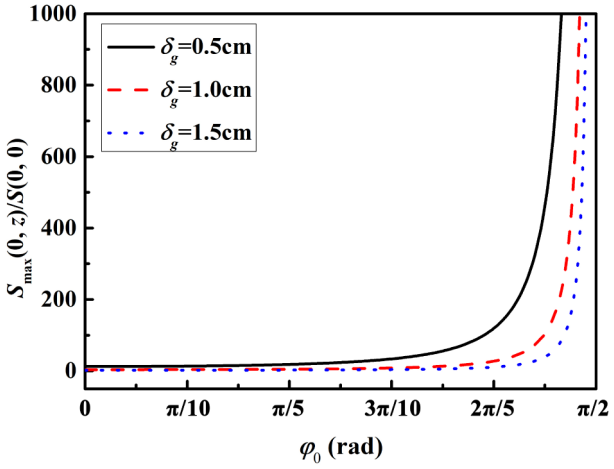

Fig. 4. The intensity ratio $S_{\max}(0, z)/S(0, 0)$ versus phase constant for different coherence length.

Figure 5 shows the evolution of the distribution of the DOC of double-H PCBs propagation in free space. In the source plane, the high-coherence area of double-H PCBs is confined to the center and two diagonal lines. As the beam propagates, the coverage of the high-coherence area reduces in the center region of the plots and increases on the two diagonals, forming side lobes. The distribution of the DOC becomes stable in the far field and it is determined by the initial beam parameter phase constant φ_0. Furthermore, the side lobes become more pronounced with large phase constant.

4.3. *Propagation in turbulent atmosphere*

Based on the summary of previous reports on PCBs propagation in turbulence, we can readily predict the evolution of the intensity and the DOC of double-H PCBs on propagation in the turbulent atmosphere. Such beams exhibit free-space diffraction properties over short distances, while at long ranges, they all degrade to a Gaussian profile eventually. The distribution of the DOC degrades to spatially quasi-homogeneous in the far field. We have verified these evolution behaviors of the intensity and the DOC of such beams with different initial beam parameters are similar, and for brevity, we just consider double-H PCBs with phase constant $\varphi_0 = 0$ and δ_g=1cm; results are shown in Fig. 6. We confirm from this figure that such beams still exhibit self-focusing in turbulence and eventually evolve to a Gaussian intensity profile. The coverage of the high-coherence area reduces gradually along one diagonal (around $\rho_1 = -\rho_2$) and the distribution of the DOC becomes spatially quasi-homogeneous, nearly constant along the diagonal lines ($\rho_2 - \rho_1$=constant) with increasing propagation distance.

With an eye towards looking at the limits of such beams for applications, we compare the effects of different initial beam parameters on the degeneration of the intensity and the DOC distributions at propagation distance $z = 4$ km in turbulence in Fig. 7. We confirm that it is difficult to judge the effect of the phase constant from the perspective of evolution of the intensity and the DOC from Fig. 7, although we seem to observe that with larger phase constant, the

Optics EXPRESS

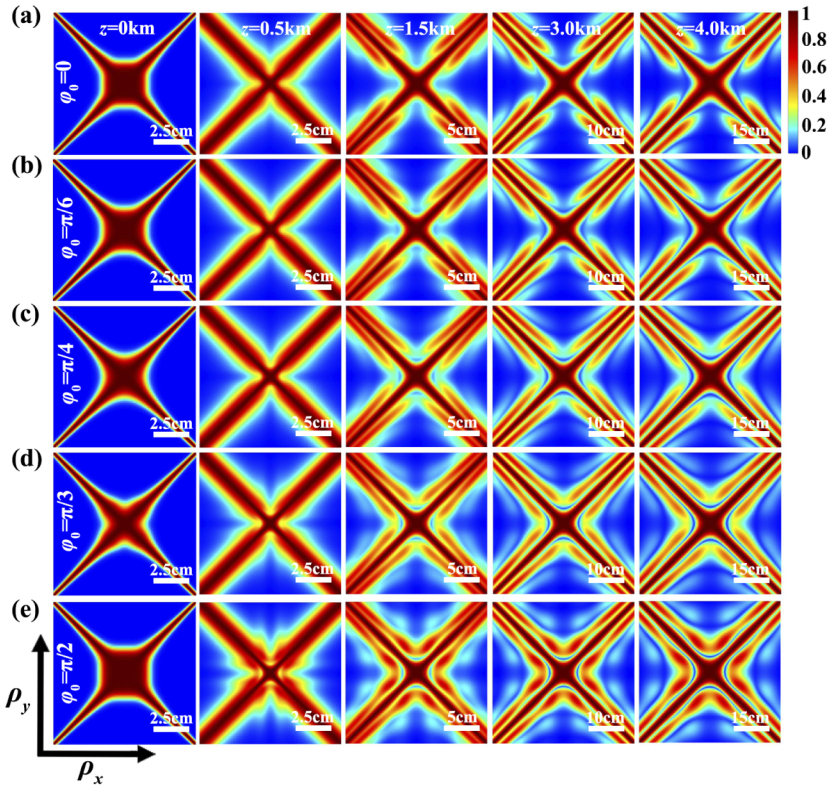

Fig. 5. Density plot of the absolute value of the DOC of double-*H* PCBs for different phase constants on propagation in free space.

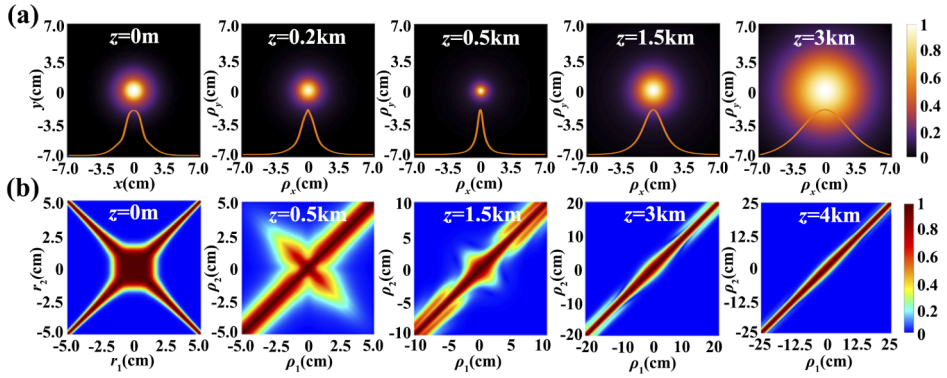

Fig. 6. The evolution of the intensity and the DOC of double-*H* PCBs on propagation in turbulence for $\varphi_0 = 0$ and δ_g=1cm.

size of the beam spot decreases slightly and the distribution of DOC degenerates to spatially quasi-homogeneous slightly slower. It cannot completely convince readers that double-*H* PCBs with large phase constant propose better turbulence resistance. Thus, we need to look for other perspectives to analyze the effect of phase constant on turbulence resistance.

Finally, we return to looking at the global parameters of double-*H* PCBs on propagation through turbulence. Figure 8 shows the evolution of the normalized propagation factor of double-*H* PCBs

Optics EXPRESS

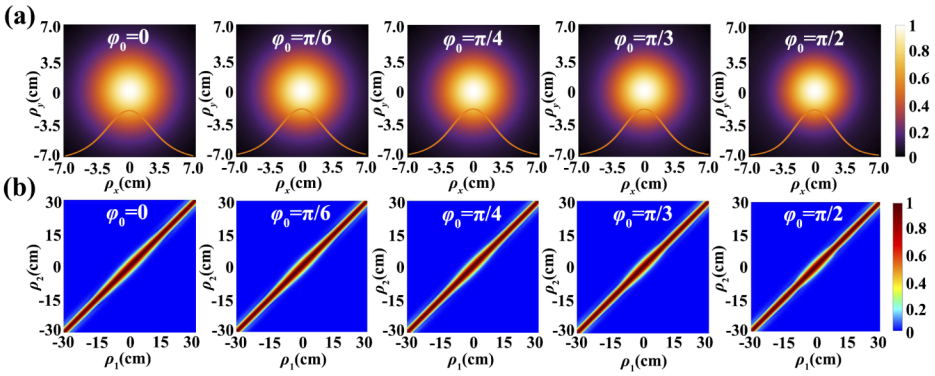

Fig. 7. Distributions of the intensity and the DOC of double-*H* PCBs for different phase constant at propagation distance z = 4km in turbulence.

on propagation in turbulence for different phase constants, and for different values of spatial coherence at a fixed propagation distance z = 3km. One confirms from Fig. 8(a) that the variation of the propagation factor on propagation in turbulence is significantly influenced by the phase constant, and the propagation factor increases more rapidly with small phase constant, which suggests that the double-*H* PCBs with large phase constants are less affected by turbulence. Furthermore, we confirm from Fig. 8(b) that the propagation factor is significantly affected by the coherence length, and that double-*H* PCBs with low coherence possess a smaller propagation factor. Therefore, we conclude from Fig. 8 that double-*H* PCBs with small phase constant and low coherence are less affected by turbulence when the propagation factor is used as a measure.

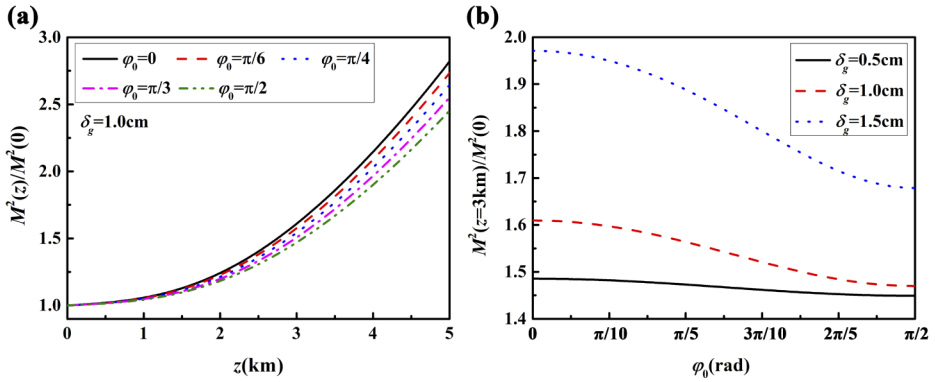

Fig. 8. Normalized propagation factors of double-*H* PCBs (a) versus propagation distance for different phase constant with δ_g = 1cm and (b) versus phase constant for different coherence length with propagation distance z = 3km.

Figure 9 shows the beam wander of double-*H* PCBs on propagation in turbulence for different phase constant, and the beam wander versus the phase constant for different coherence lengths at certain propagation distance at z = 3km. It is found that the evolution of the beam wander curve is similar to that of propagation factor. The double-*H* PCBs with large phase constant and low coherence experience smaller beam wander. Therefore, from the perspective of beam wander, we once again find that double-*H* PCBs with large phase constant and low coherence are less affected by turbulence.

Optics EXPRESS

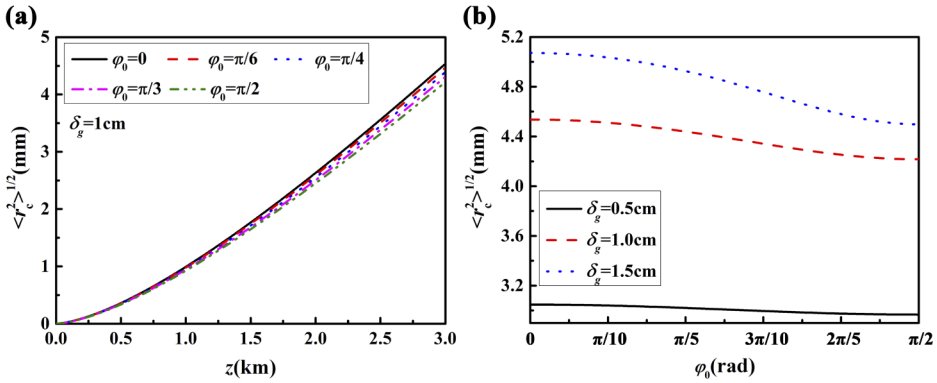

Fig. 9. Beam wander of double-*H* PCBs (a) versus propagation distance for different phase constant and (b) versus phase constant for different coherence length with certain propagation distance z = 3km.

5. Summary and observations

We have studied the statistical properties of double-*H* PCBs in the source plane and on propagation in free space and turbulence. It is found that the statistical properties of such beams are quite different from those of single-*H* PCBs. We have shown that the beam profile of double-*H* PCBs in the source plane can be modulated by adjusting the phase constant and coherence. Double-*H* PCBs display self-focusing propagation properties both in free space and in turbulence. Furthermore, such beams with large phase constant and low coherence are less affected by turbulence than such beams with small phase constant and high coherence.

It is worthwhile to say a few words about the physics that leads such beams to have their unusual statistical properties. As seen by Eq. (4), double-*H* sources can be viewed as a superposition of two sources, one is a NUC source and another one is a modulated NUC source. Therefore, the intensity distribution of double-*H* sources is either the constructive or destructive combination of these two sources when $\varphi_0<\pi/4$ and $\varphi_0>\pi/4$, respectively; the phase constant plays a critical role in the behavior of the field. NUC beams display a self-focusing property both in free space and in turbulence, which had been discussed in Ref. [22,29], while modulated NUC beams diverges rapidly on propagation. Therefore, double-*H* PCBs gradually exhibit the characteristics of NUC beams, i.e. self-focusing property, on propagation. We can also explain the evolution of propagation factor and beam wander of such beams in turbulence from this perspective. The influence of the modulated NUC beams on the propagation factor and beam wander are negative and reductive when phase constants increase from 0 to $\pi/4$, and they are positive and incremental when phase constants increase from $\pi/4$ to $\pi/2$. Therefore, double-*H* PCBs with large phase constant display better turbulence resistance.

Our results of the study on the propagation properties of this new class of double-*H* PCBs shows that beams with a superposition of two or more beam modes have new degrees of freedom, such as the phase constant, and that we can adjust the weight of the beam modes to show novel propagation properties and better turbulence resistance, which can be tailored for the individual application needs. This flexibility can be used to improve the characteristics of beams in free-space optical communications.

Funding. National Key Research and Development Program of China (2019YFA0705000); National Natural Science Foundation of China (11525418, 11904087, 11947240, 12004218, 1750201); China Postdoctoral Science Foundation (2020M680093); Natural Science Foundation of Shandong Province (ZR2020QA067); Local Science and Technology Development Project of the Central Government (YDZX20203700001766); Innovation Group of Jinan (2018GXRC010).

Disclosures. The authors declare no conflicts of interest.

Optics EXPRESS

Data availability. All data that support the findings of this study are included within the article.

References

1. E. Wolf, "Coherence and radiometry," J. Opt. Soc. Am. **68**(1), 6–17 (1978).
2. E. Wolf and D. F. V. James, "Correlation-induced spectral changes," Rep. Prog. Phys. **59**(6), 771–818 (1996).
3. D. F. V. James, "Change of polarization of light beams on propagation in free space," J. Opt. Soc. Am. A **11**(5), 1641 (1994).
4. E. Wolf, "Correlation-induced changes in the degree of polarization, the degree of coherence, and the spectrum of random electromagnetic beams on propagation," Opt. Lett. **28**(13), 1078 (2003).
5. L. Mandel and E. Wolf, *Optical coherence and quantum optics* (Cambridge University, 1995).
6. D. Peng, Z. Huang, Y. Liu, Y. Chen, F. Wang, S. A. Ponomarenko, and Y. Cai, "Optical coherence encryption with structured random light," PhotoniX **2**(1), 6–15 (2021).
7. O. Korotkova and G. Gbur, "Applications of optical coherence theory," Prog. Opt. **65**, 43–104 (2020).
8. G. Gbur and E. Wolf, "Spreading of partially coherent beams in random media," J. Opt. Soc. Am. A **19**(8), 1592–1598 (2002).
9. G. Gbur, "Partially coherent beam propagation in atmospheric turbulence (invited)," J. Opt. Soc. Am. A **31**(9), 2038–2045 (2014).
10. G. A. Dogariu and S. Amarande, "Propagation of partially coherent beams:turbulence-induced degradation," Opt. Lett. **28**(1), 10–12 (2003).
11. T. Shirai, A. Dogariu, and E. Wolf, "Mode analysis of spreading of partially coherent beams propagating through atmospheric turbulence," J. Opt. Soc. Am. A **20**(6), 1094–1102 (2003).
12. Y. Cai, Y. Chen, J. Yu, X. Liu, and L. Liu, "Generation of partially coherent beams," Prog. Opt. **62**, 157–223 (2017).
13. F. Gori and M. Santarsiero, "Devising genuine spatial correlation functions," Opt. Lett. **32**(24), 3531–3533 (2007).
14. Y. Cai, Y. Chen, and F. Wang, "Generation and propagation of partially coherent beams with nonconventional correlation functions: a review [Invited]," J. Opt. Soc. Am. A **31**(9), 2083–2096 (2014).
15. J. Yu, X. Zhu, S. Lin, F. Wang, G. Gbur, and Y. Cai, "Vector partially coherent beams with prescribed non-uniform correlation structure," Opt. Lett. **45**(13), 3824–3827 (2020).
16. F. Wang, X. Liu, Y. Yuan, and Y. Cai, "Experimental generation of partially coherent beams with different complex degrees of coherence," Opt. Lett. **38**(11), 1814–1816 (2013).
17. M. Hyde, S. Bose-Pillai, D. Voelz, and X. Xiao, "Generation of Vector Partially Coherent Optical Sources Using Phase-Only Spatial Light Modulators," Phys. Rev. Appl. **6**(6), 064030 (2016).
18. M. Hyde, S. Bose-Pillai, and R. A. Wood, "Synthesis of non-uniformly correlated partially coherent sources using a deformable mirror," Appl. Phys. Lett. **111**(10), 101106 (2017).
19. M. Hyde, "Generating electromagnetic Schell-model sources using complex screens with spatially varying auto-and cross-correlation functions," Results Phys. **15**, 102663 (2019).
20. X. Zhu, J. Yu, Y. Chen, F. Wang, and Y. Cai, "Experimental synthesis of random light sources with circular coherence by digital micro-mirror device," Appl. Phys. Lett. **117**(12), 121102 (2020).
21. Y. Yuan, T. Lei, S. Gao, X. Weng, L. Du, and X. Yuan, "The Orbital Angular Momentum Spreading for Cylindrical Vector Beams in Turbulent Atmosphere," IEEE Photonics J. **9**(2), 1–10 (2017).
22. H. Lajunen and T. Saastamoinen, "Propagation characteristics of partially coherent beams with spatially varying correlations," Opt. Lett. **36**(20), 4104–4106 (2011).
23. L. C. Andrews and R. L. Phillips, *Laser Beam Propagation through Random Media* (SPIE, 2005).
24. I. Toselli, L. C. Andrews, R. L. Phillips, and V. Ferrero, "Free-space optical system performance for laser beam propagation through non-Kolmogorov turbulence," Opt. Eng. **47**(2), 026003 (2008).
25. Y. Dan and B. Zhang, "Second moments of partially coherent beams in atmospheric turbulence," Opt. Lett. **34**(5), 563–565 (2009).
26. R. Martínez-Herrero, P. M. Mejías, and G. Piquero, "Quality improvement of partially coherent symmetric-intensity beams caused by quartic phase distortions," Opt. Lett. **17**(23), 1650–1651 (1992).
27. X. Xiao and D. Voelz, "Beam wander analysis for focused partially coherent beams propagating in turbulence," Opt. Eng. **51**(2), 026001 (2012).
28. J. Yu, F. Wang, L. Liu, Y. Cai, and G. Gbur, "Propagation properties of Hermite non-uniformly correlated beams in turbulence," Opt. Express **26**(13), 16333–16343 (2018).
29. Z. Mei and D. Zhao, "Controllable dark-hollow beams and their propagation characteristics," J. Opt. Soc. Am. A **22**(9), 1898 (2005).
30. R. Martínez-Herrero, G. Piquero, and P. M. Mejías, "Beam quality changes of radially and azimuthally polarized fields propagating through quartic phase plates," Opt. Commun. **281**(4), 756–759 (2008).